Unveiling causal relationship between non-covalent interactions and evaluated Young's modulus within oligolignols-cellulose complexes

Pablo Lopez Albarran [Corresp., Equal first author, 1], **Rafael Herrera-Bucio** [Equal first author, 2], **Antonio Pizzi** [3], **Joel A. Sanchez-Badillo** [Corresp., 1], **Marco Gallo** [4], **Raymundo Hernández-Esparza** [5], **Jorge Garza** [6]

[1] Facultad de Ingenieria en Tecnologia de la Madera, Universidad Michoacana de San Nicolás de Hidalgo, Morelia, Michoacan, Mexico

[2] Instituto de Investigaciones Quimico Biologicas, Universidad Michoacana de San Nicolás de Hidalgo, Morelia, Michoacan, Mexico

[3] ENSTIB École Nationale Supérieure des Technologies et Industries, Université de Lorraine, Epinal, Lorraine, France

[4] Campus Instituto Tecnológico de Ciudad Juárez, Tecnologico Nacional de Mexico, Ciudad Juarez, Chihuahua, Mexico

[5] Leadership Computing Facility, Argonne National Laboratory, Lemont, Illinois, Unites States of America

[6] Division de Ciencias Basicas e Ingenieria - Departamento de Quimica, Universidad Autonoma Metropolitana Unidad Iztapalapa, Mexico, Mexico, Mexico

Corresponding Authors: Pablo Lopez Albarran, Joel A. Sanchez-Badillo
Email address: plopez@umich.mx, joel.sanchez@umich.mx

Linear correlations coefficients were calculated between the reported Young's modulus values and non-covalent interactions within cellulose-oligolignol complexes, considering the composition of an efficient adhesive formulation as previously reported. A paradigmatic relationship was observed. Molecular complexes of oligolignols with cellulose Iβ were modeled using hybrid quantum mechanics/molecular mechanics (QM/MM) computations to obtain wavefunctions at the interaction region. Subsequently, a study of non-covalent interactions (NCI) based on the atoms in molecules (AIM) theory was implemented, utilizing graphics processing units (GPUs) for calculations. Our findings indicate that non-covalent interactions control the forces associated to adhesive-cellulose contacts, primarily through C-H···O hydrogen bonds, which promote the adhesion of oligolignols on cellulose Iβ. Significant linear correlations were observed between reported values Young's modulus and the molecular interactions observed, rendering the influence of oligolignol structure on the adhesion phenomenon in our cellulose Iβ crystallite model. These observations promote the NCI and AIM analysis in a new framework to design adhesive formulations.

Unveiling causal relationship between non-covalent interactions and evaluated Young's modulus within oligolignols-cellulose complexes.

Pablo López-Albarrán,[*1] Rafael Herrera-Bucio,[2] Antonio Pizzi,[3] Joel A. Sánchez-Badillo,[1] Marco Gallo,[4] Raymundo Hernández-Esparza,[5] and Jorge Garza[6]

[1] Facultad de Ingeniería en Tecnología de la Madera, Universidad Michoacana de San Nicolás de Hidalgo, Morelia, Michoacán, 58030, México.
[2] Instituto de Investigaciones Quimico Biologicas, Universidad Michoacana de San Nicolás de Hidalgo, Morelia, Michoacan, Mexico
[3] Ecole Nationale Supérieure des Technologies et Industries du Bois (ENSTIB), Université de Lorraine, France.
[4] Tecnológico Nacional de México/ITCJ, Cd. Juárez, Chihuahua, 32500, México.
[5] Leadership Computing Facility, Argonne National Laboratory, 9700 S. Cass Avenue, Lemont, IL 60439, USA.
[6] Departamento de Química, Universidad Autónoma Metropolitana – Iztapalapa, Iztapalapa., México.

Corresponding Authors:
Pablo López-Albarrán[1]
email address: plopez@umich.mx
Joel A. Sánchez-Badillo[1]
email address: joel.sanchez@umich.mx

Abstract

Linear correlation coefficients were calculated between the reported Young's modulus values and non-covalent interactions within cellulose-oligolignol complexes, considering the composition of an efficient adhesive formulation as previously reported. A paradigmatic relationship was observed. Molecular complexes of oligolignols with cellulose Iβ were modeled using hybrid quantum mechanics/molecular mechanics (QM/MM) computations to obtain wavefunctions at the interaction region. Subsequently, a study of non-covalent interactions (NCI) based on the atoms in molecules (AIM) theory was implemented, utilizing graphics processing units (GPUs) for calculations. Our findings indicate that non-covalent interactions control the forces associated to adhesive-cellulose contacts, primarily through C-H···O hydrogen bonds, which promote the adhesion of oligolignols on cellulose Iβ. Results indicate that the adhesion strength projected from larger YM values cannot be describe solely by the number of stronger hydrogen bonds nor by the number of the weak interactions but by the entire contributions of

specific interactions. Thus, significant linear correlations were observed between reported values Young's modulus and the molecular interactions observed, rendering the influence of oligolignol structure on the adhesion phenomenon in our cellulose Iβ crystallite model. These observations promote the NCI and AIM analysis in a new framework to design adhesive formulations.

Introduction

The need for eco-friendly wood adhesives has led to intense research on adhesives derived from natural and non-toxic materials (Pizzi, 2006, 2013; Antov, Savov & Neykov, 2020) Several studies have been reported on this topic, considering the lignin as one of the raw materials at the forefront of such studies (Nimz, 1983; Pizzi, 1994; Imam et al., 2001; Desai, Patel & Sinha, 2003; Li et al., 2004). On this context, the oligolignol-composition and Young's modulus (YM) experimental values from lignin-based adhesives, were postulated and identified by MALDI-TOF (matrix assisted laser desorption ionization time-of-flight) mass spectroscopy (Sedano-Mendoza, Lopez-Albarran & Pizzi, 2010a). In that study, a computational molecular docking analysis was employed to establish a correlation between the interaction energy of the proposed adhesives and a cellulose Iβ crystallite model. These interaction energies were directly associated with the experimental YM values obtained through thermomechanical analysis (Martinez et al., 2010). The reported correlations in the study were considered acceptable. However, certain adhesive mixtures exhibited low correlation factors, despite their YM values implying effective adhesion. Naturally, the utilization of a molecular docking methodology serves as an initial approach to understand the interactions involved in the oligolignol-cellulose contact.

Recently, we developed Reactive Force Field (ReaxFF) (Chenoweth, Van Duin & Goddard, 2008) molecular dynamic simulations to elucidate the contribution of each oligolignol's molecular structure to the adhesive capacity of the lignin mixture. We modelled the interaction of each oligolignol with a cellulose Iβ crystallite model (López-Albarrán et al., 2017). The important results from those simulations were the coupling energies obtained for the oligolignol-cellulose complexes, which correlate quite well with experimental values of their Young's modulus. However, an *ab-initio* study is required to elucidate which molecular interactions are involved in the oligolignols-cellulose complexes, to determine which interactions address the adhesion effect beyond the energetic description.

The intermolecular contacts between cellulose and adhesives constitute an important research area due to their potential in designing non-toxic glues for the wood industry (Fengel & Wegener, 1983; Houtman & Atalla, 1995; Imam et al., 2001; Desai, Patel & Sinha, 2003; Chenoweth, Van Duin & Goddard, 2008). Hydrogen bonding is undoubtedly a crucial topic for experimental and theoretical researchers (Nishiyama, Langan & Chanzy, 2002a; Ishikawa et al., 2015), as this interaction plays a key role in stabilizing the cellulose network (Moon et al., 2011; Djahedi et al., 2016). However, several authors (Cintrón, Johnson & French, 2011; Huang et al., 2021) have emphasized the need for careful consideration of both strong and weak hydrogen bonds, as these interactions offer insights into the design of materials with desired mechanical

properties. Unfortunately, *ab-initio* studies demand extensive computational time due to the large size of the systems involved.

In the composition of lignocellulosic biomass, lignin is a major component of wood, second only to cellulose, and acts as a cementing agent among wood cells.(Fengel & Wegener, 1983) Extensive research from the scientific and engineering perspectives has been developed to investigate the interaction between cellulose and lignin, aiming to design and develop novel wood adhesive formulations (Pizzi, 1994; Pizzi & Mittal, 2011). The inclusion of lignin in these formulations has shown adhesive properties similar to those of phenol-formaldehyde resins (Jin, Cheng & Zheng, 2010; Pizzi, 2013), which find widespread application in industries involved in particleboard, plywood, fiberboard, and laminated wood (Navarrete et al., 2010; Mansouri et al., 2011)

Empirical studies have conducted on lignin-based adhesives (Knop & Scheib, 1979; Nimz, 1983). However, these studies have overlooked the molecular mechanism and the atomistic interactions within the cross-linked structure of lignin, specifically 4-hydroxyphenylpropanoids. Consequently, the driving forces behind the adhesion phenomenon remain unclear. Moreover, classical molecular dynamics simulations have been performed to investigate the absorption of lignin onto various cellulose surfaces (Besombes & Mazeau, 2005). Although the energy of interactions between lignin and cellulose has been reported, specific interactions relevant to adhesiveness, Young's modulus, or mechanical properties have not been addressed.

The lignin structure is primarily composed of simple units of 4-hydroxyphenylpropane, specifically three hydroxycinnamyl alcohols: p-coumarol, coniferol, and sinapol (Fig. 1). These units are commonly referred to as monolignols (Fengel & Wegener, 1983).

Figure 1. Lignin precursors. (A) p-coumarol, (B) coniferol, and (C) sinapol, all of them showed in their predominant (E)-monolignol configuration. Carbon numbering is shown on the coniferol structure.

In general, coniferol units are more abundant in softwood than in hardwood, as the latter exhibits a comparable proportion of coniferol and sinapol units (Shimada & Higuchi, 1983). The composition of lignin in solution differs from that of native lignin (protolignin) found in wood, owing to the extraction process (Terashima, Nakashima & Takabe, 1998). Despite these differences, the most abundant linkages observed between lignin units are as follows: *β-O-4'* (*βO4*), *β-5'* (*β5*) and *β-β'* (*ββ*) (Sjöström, 1998).

In this work, we propose an atomistic analysis to investigate the role of the molecular structures of oligolignols in the adhesion properties of lignin-based formulations, as determined by Young's modulus. These structures have previously been characterized using the MALDI-TOF technique. Molecular dynamics simulations employing the ReaxFF are performed to model the coupling behavior of oligolignols on a cellulose Iβ crystallite. Subsequently, a hybrid quantum mechanics/molecular mechanics (QM/MM) (Vreven & Morokuma, 2006) study is applied to

examine the obtained coupled molecular geometries of the oligolignol-cellulose complexes derived from the molecular dynamics study. Each complex is re-optimized to refine its conformation, which is then utilized to calculate its electron density ($\rho(\boldsymbol{r})$) through density functional theory (DFT) (Kohn, Becke & Parr, 1996). The structures are subsequently analyzed using two tools developed within the quantum chemistry: 1) The non-covalent interaction index (NCI) (Johnson et al., 2010a), which explores regions where possible non-covalent interactions are present, and 2) the atoms in molecules (AIM) theory (Bader & Nguyen-Dang, 1981) which is a useful approach based on the electronic density ($\rho(\boldsymbol{r})$) distribution within molecules in order to describe possible inter and intra non-covalent bonds. The NCI provides information on regions of non-covalent interactions, such as hydrogen bonds, weak interactions, and steric clashes, by evaluating the reduced gradient of the electron density (Boto et al., 2016), which is defined as:

$$s(\boldsymbol{r}) = \frac{1 \quad |\nabla\rho(\boldsymbol{r})|}{2\left(3\pi^2\right)^{\frac{1}{3}} \; \rho(\boldsymbol{r})^{\frac{4}{3}}} \tag{1}$$

Therefore, the determination of electron density and its derivatives are essential for the NCI assessment. Furthermore, the identification of critical points $(\boldsymbol{r}_c)$ in the electron density, $\rho(\boldsymbol{r}_c)$, plays a crucial role in the AIM approach. Accordingly, the identification of $\boldsymbol{r}_c$ satisfying the Laplacian $\nabla\rho(\boldsymbol{r}_c) = 0$ is important for the analysis of the electron density as these points indicate bond paths and bond critical points. Thus, these quantum chemistry tools serve to describe and elucidate both short- and long-range interactions involved in the adhesion of oligolignols to the cellulose Iβ surface. Evidently, the aim of this work is to stablish a foundation for designing and developing adhesive formulations for lignocellulosic materials by gaining insight into their fundamental molecular interactions with a cellulose Iβ surface. As far as we know, no previous theoretical reports have employing reactive molecular dynamics in conjunction with NCI-AIM methodologies to elucidate the interaction between oligolignols and cellulose. This research represents a key step towards the development of new and eco-friendly adhesive formulations for wood.

Naturally, performing NCI-AIM evaluations along with their corresponding derivatives can be a challenging when dealing with considerable systems sizes. To address this issue, we employ the GPUAM code, a QM program specifically designed to handle large systems and optimized for graphics processing units (GPUs) (Hernández-Esparza et al., 2014). GPUAM has demonstrated its capability to deliver reliable results in less computing time compared to software developed for x86 multicore CPUs (Hernández-Esparza et al., 2014).

We believe that this type of study provides a framework for elucidating oligolignols or lignin substructures within lignin-adhesive formulations that augment cellulose adhesion. Besides, the present study can contribute to delineating the interactions between lignin components and cellulose.

Materials & Methods

Considering that the most prevalent form of the cellulose in higher plants is cellulose Iβ (Nishiyama, Langan & Chanzy, 2002b), the cellulose model used in this work was constructed based on crystalline structures characterized through X-ray and neutron fiber diffraction measurements (Nishiyama, Langan & Chanzy, 2002a; Nishiyama et al., 2003). Our cellulose Iβ crystallite model comprises three layers in the y direction and six glucan chains in the z direction. Each chain consists of 12 glucose units (equivalent to six cellobioses) in the x direction, as illustrated in Fig. 2.

Figure 2. Snapshot of the cellulose Iβ model used to form the complexes with the oligolignols. The model was built using the Cellulose-Builder toolkit (Gomes & Skaf, 2012), and visualized by the Vesta molecular viewer (Momma & Izumi, 2008). Color key: carbons atoms are in dark-gray, oxygen atoms in red, and hydrogen atoms in white.

The molecular structures of oligolignols elucidated by our MALDI-TOF experimental results, were constructed using the ChemBioOffice Ultra software version 11.0.1 (Ultra, 2007). These oligolignols were assumed to interact with the cellulose Iβ crystallite model. The set of oligolignols examined in this study (see Fig. 3) was characterized from the experimental adhesive formulation with the best performance (highest value for Young's modulus) (Pizzi et al., 2011). As observed, the modeled oligolignols are constituted only by coniferyl (Fig. 1B) and sinapyl (Fig. 1C) units. We employed the following nomenclature for oligolignols: A_m_B_n_C where A, B or C indicates a coniferyl (CA) or sinapyl (SA) alcohol linked by one m or n linkage (for instance, βO4, ββ, and β5). Therefore, we constructed the following oligolignols CA_βO4_SA_β5_CA (Fig. 3A), CA_βO4_SA_ββ_SA (Fig. 3B), SA_βO4_SA_ββ_SA (Fig. 3C), and CA_ββ_CA (Fig. 3D).

Figure 3. Molecular structures of the oligolignols in the reported efficient adhesive formulation. (A) CA_βO4_SA_β5_CA, (B) CA_βO4_SA_ββ_SA, (C) SA_βO4_SA_ββ_SA, and (D) CA_ββ_CA.

The present Quantum Mechanics (QM)/Molecular Mechanics (MM) study utilized the four oligolignol-cellulose complexes previously reported in the most effective oligolignol-mixture (Sedano-Mendoza, Lopez-Albarran & Pizzi, 2010b; López-Albarrán et al., 2017). The study employed the ONIOM method (Dapprich et al., 1999), implemented in the Gaussian16 suite code (Frisch et al., 2016). This methodology enables the analysis of the primary interactions using an *ab-initio* approach. In our proposed approach, the QM region comprised the oligolignol and a cellulose Iβ surface fragment, while the remainder of the cellulose model was designated as the MM region. The four oligolignol-cellulose complexes were geometrically minimized applying the ONIOM method which defines two or three layers (molecular or atomic) within the

structure that are evaluated at different levels of molecular modeling. The geometry optimization for each complex, was performed including long range interactions by using the CAM-B3LYP (Yanai, Tew & Handy, 2004) method and the cc-pVDZ Dunning (Kendall, Dunning Jr & Harrison, 1992) basis set. The MM contribution was calculated applying the universal force field (UFF) (Rappé et al., 1992) implemented in the Gaussian16 suit package. The output coordinates obtained from the QM/MM minimization process were employed to compute the electronic wavefunction via a single point energy calculation for the QM region (oligolignol and part of the cellulose complex). These calculations were carried out considering that the QM region requires an *ab-initio* method or methods developed to describe van der Waals (vdW) interactions. In this work, the M06-2X functional (Zhao & Truhlar, 2008), including dispersion interactions proposed by Grimme in the commonly form named "D3"(Grimme, 2004), was used for vdW corrections. Recently, different Kohn–Sham approaches have been employed to test the behavior of some cellulose properties by including dispersion interactions in periodic systems (Navarrete-López, San-Román & Zicovich-Wilson, 2016). The resulting wavefunction was then analyzed to evaluate the NCI interactions associated with the AIM approach for each system. The evaluation of NCI index and the bond critical points related to AIM theory, were obtained by using a grid-based method. This grid-based method was developed and implemented by Hernández-Esparza et al. on graphics processing units (GPUs), which is quite convenient to reduce considerably the computation efforts, particularly in large systems, such as the oligolignol-cellulose complexes studied in this manuscript. Subsequently, the observed interactions were classified into $_{adh}OH\cdots O_{Cell}$, $_{adh}O\cdots HO_{Cell}$, $_{adh}CH\cdots O_{Cell}$, $_{adh}O\cdots HC_{Cell}$, $_{adh}C\pi H\cdots O_{Cell}$, and $_{adh}C\pi\cdots HC_{Cell}$, based on its electron density and the Laplacian of the electron density (which must be positive for all cases). Among them, weak interactions were considered as all of interactions with electron density value less than 0.005 a.u. (Johnson et al., 2010a). Finally, a series of correlations between the observed interactions and the previously reported experimental values for the Young's modulus were determined.

Results

The molecular structures of the oligolignol-cellulose complexes optimized at the interaction region through the QM/MM-ONIOM studies, remain almost in the same conformation than those obtained from our previous LAMMPS-ReaxFF-MD study (López-Albarrán et al., 2017). The superposition of the obtained oligolignols conformations in this QM/MM study against those reported from our LAMMPS-ReaxFF-MD simulations, is displayed in Fig. 4. The cellulose model was not displayed, to facilitate visualization; however, the entire system is displayed in Fig. S1. Additionally, the QM and MM regions for each oligolignol-cellulose complexes are displayed in the Fig. S2 in the Supplemental Information.

Figure 4. Superposition of the four oligolignols complexed over the cellulose Iβ crystallite model. For convenience the cellulose Iβ surface is not present in this figure however, this part of

the system was considered in the QM/MM optimization process. The complex conformations obtained from the LAMMPS-ReaxFF-MD are in green carbon-skeleton, and the QM/MM-CAM-B3LYP(Yanai, Tew & Handy, 2004)/cc-pVDZ(Kendall, Dunning Jr & Harrison, 1992)/Universal Force Field(Rappé et al., 1992) (UFF) are in purple carbon-skeleton. (A) CA_*βO4*_SA_*β5*_CA trilignol, (B) CA_*βO4*_SA_*ββ*_SA trilignol, (C) SA_*βO4*_SA_*ββ*_SA trilignol, and (D) CA_*ββ*_CA dilignol.

The molecular interactions arising from the adhesion between the cellulose Iβ crystallite model and each oligolignol were analyzed using NCI-AIM surfaces to establish relationships between these interactions and the Young's modulus. The intermolecular interactions are presented in Fig. 5, with only QM regions displayed. The localization of the NCIs through the surfaces was related to the reduced gradient density (RGD) plot regions, similar to the approach by Ponnuchamy, Sandak & Sandak, (2020). Due to the absence of steric clashes (red isosurfaces), adhesion is promoted by attractive non-covalent interactions (green and blue isosurfaces).
In Fig. 5A, the CA_βO4_SA_β5_CA-cellulose Iβ complex shows strong interactions (blue isosurfaces) labeled as **a**-**d**. The system also displays relative weak interactions with electron density values around 0.011 a.u. (labels **e**-**j**). Additionally, there are large green isosurfaces with small electron density values (<0.002 a.u., labeled as **l** and **m**). Strong hydrogen bonds labeled as **a** and **b** are found in the CA_βO4_SA_ββ_SA-cellulose Iβ complex (Fig. 5B). Moreover, localized contacts (small green isosurfaces related two atoms) are indicated with **c**-**f**, **j**, **m**, **n** and **q**-**s** labels. These interactions span a range from ~0.001 a.u to ~0.015 a.u.
In the case of SA_βO4_SA_ββ_SA-cellulose Iβ complex in Fig. 5C, one strong hydrogen bond is noticeable, as indicated by the **a** label. Localized contacts are indicated with **b**-**d**, **f**, **g**, **k**, **q**, **s**, **t**, and **u** labels in the range ~0.001 a.u. to 0.012 a.u. Interestingly, this number of interactions is similar but weaker than those found in Complex 2. Finally, for the CA_ββ_CA-cellulose Iβ (Fig. 5D), despite the lower number of interactions compared to previous systems, the localized **b**, **c**, and **e** contacts extend over a narrower but stronger 0.003 a.u. to 0.012 a.u. range compared to the remaining complexes.

Figure 5. Mapping of the NCI-AIM surfaces and plot of reduced electron density gradient (RDG) against Sign(λ_2)ρ. (A) Complex 1, CA_*βO4*_SA_*β5*_CA– cellulose Iβ; (B) Complex 2, CA_*βO4*_SA_*ββ*_SA–cellulose Iβ; (C) Complex 3, SA_*βO4*_SA_*ββ*_SA–cellulose Iβ; (D) Complex 4, CA_*ββ*_CA–cellulose Iβ. Blue regions are for hydrogen bonds, green regions for van der Waals. The gradient isosurfaces correspond to a cutoff of 0.5 a.u. Color scale ranging from $-0.4 < \rho < 0.4$ a.u. The interactions labeled as **a**-**u** (if exist) corresponded to the interactions indicated in Tables S1-S4.

Additionally, the AIM approach was used to determine possible (localized) contacts between atoms from oligolignols and atoms from the cellulose surface, through bond paths. These bond

paths are displayed in Fig. 6 for each oligolignol-cellulose complex. By analyzing bond paths, a series of hydrogen bonds: O-H···O, C-H···O and Cπ-H···O were found. These hydrogen bonds presented electronic density values between 0.006 and 0.040 a.u., accordingly to the electronic density criterion from Johnson et al.(Johnson et al., 2010a) A detailed analysis of these contacts, including weak interactions, is presented in Tables S1 to S4 in the Electronic Supplemental Information.

Figure 6. Illustration of the main hydrogen bond based on electronic density isovalues and a blue code color: $\boldsymbol{\rho(r) \geq 0.02}$ in dark blue, $\boldsymbol{0.01 \leq \rho(r) < 0.02}$ in blue and $\boldsymbol{\rho(r) < 0.01}$ in cyan.(Johnson et al., 2010b) Atoms involved in hydrogen bond are highlighted in magenta. (A) Complex 1, CA_*βO4*_SA_*β5*_CA – cellulose Iβ; (B) Complex 2, CA_*βO4*_SA_*ββ*_SA – cellulose Iβ; (C) Complex 3, SA_*βO4*_SA_*ββ*_SA – cellulose Iβ; (D) Complex 4, CA_*ββ*_CA – cellulose Iβ.

Discussion

The adhesion process for each complex is driven by non-covalent interactions, as evidenced by the occurrence of both small and large green zones between oligolignol and cellulose fragments with few blue zones (typically labeled as **a-d** in Fig. 5), indicative of strong hydrogen bonds (Johnson et al., 2010a). Although these interactions may appear covalent at first glance due to strong binding, like previous reports where strong hydrogen bonds stabilize DNA base pairs (Jurečka et al., 2006), it is important to note that they are, in fact, non-covalent in nature.
The significance of $\rho(\boldsymbol{r})$ values is acknowledged, with larger values corresponding to greater binding energies for hydrogen bonds (Koch & Popelier, 1995; Navarrete-López, Garza & Vargas, 2007). However, it is not easy to know the contribution of each contact to the binding energy. Naturally, the possible cooperativity exhibited by hydrogen bonds in these systems is one important topic to be analyzed in future studies. In addition, the many-body problem involved in the lignin-cellulose interaction is one important factor that is not addressed in this report and our conclusions are limited by the QM/MM model. For that reason, it is not possible to compare one to one binding energies from QM with ReaxFF-MD. Notwithstanding these limitations, the non-covalent interaction (NCI) interactions depicted in Fig. 5, and the bond paths reported in Fig.6 offer valuable insights. The examination of these interactions may unveil potential connections between the macroscopic Young's modulus values and the specific punctual interactions arising after the contact between cellulose and oligolignol. In this context, the study aims to elucidate the atomistic interactions or their interconnections governing the adhesion phenomenon through YM. Such interactions can validate the influence of oligolignols composition and contribute to the synthesis of efficient adhesive formulations.
The reported YM values among the four oligolignols from the best tested depolymerized lignin, shown the following order for the optimal adhesion between oligolignols and cellulose Iβ:

CA_βO4_SA_ββ_SA(0.3011 MPa)>CA_ββ_CA(0.2988 MPa)>SA_βO4_SA_ββ_SA(0.2093 MPa)>CA_βO4_SA_β5_CA(0.1346 MPa) (Sedano-Mendoza, Lopez-Albarran & Pizzi, 2010b). The trilignol with the lowest YM value exhibited inefficient adhesion, as elucidated by our NCI-AIM study. The CA_βO4_SA_β5_CA trilignol did not achieved optimal coupling over the cellulose Iβ crystallite model, yielding complexes that do not promote adhesion. One reason may be that the trilignol exhibits folding (see Fig. 5A), reducing intermolecular non-covalent interactions. This conformation produces large green isosurfaces related to non-localized contacts. Interestingly, this oligolignol present the strongest hydrogen bonds (**a** and **b** interactions located at electron density values of 0.04 and 0.038 a.u., respectively) but also the lowest YM value (0.1346 MPa). In contrast, the CA_βO4_SA_ββ_SA trilignol shows optimal coupling on the cellulose Iβ crystallite, reducing the large isosurfaces and increasing the localized non-covalent interactions (**a**-**s**), as shown in Fig. 5B. This combined effect promotes oligolignol adhesion due to the occurrence of several both hydrogen bonds and weak interactions towards the cellulose crystallite, see Table S2. It is noteworthy that, despite producing the largest YM value, the CA_βO4_SA_ββ_SA trilignol has weaker hydrogen bonds and a large number of weak interactions compared to those found in Complex 1. Similar coupling is observed for the SA_βO4_SA_ββ_SA–cellulose Iβ complex, shown in Fig. 5C. However, it presents weaker hydrogen bonds and a small number of weak interactions (see Table S3).

Finally, the CA_ββ_CA dilignol achieves efficient adhesion due to its large YM value (Sedano-Mendoza, Lopez-Albarran & Pizzi, 2010b). From the NCI-AIM analysis, it was found that this dilignol displays a relatively low number of weak non-covalent interactions; however, they are concentrated in a narrow range, as can be seen from Table S4 and indicated previously. Moreover, the dilignol did not show strong hydrogen bonds, as the plot of reduced electron density gradient (RDG) against Sign(λ2)ρ suggests, shown in Fig. 5D. However, experimental and theoretical results from the literature support that the CA_ββ_CA oligolignol is the second-best lignin substructure contributing to the adhesion (Mansouri et al., 2011), as it was the unique substructure plausible to couple more dilignols over the cellulose surface.

The previous analysis suggests that both weak non-covalent interactions and hydrogen bonds likely play a complementary role in mechanical properties such as Young's modulus. To explore this effect further, the reported interactions were classified, and their respective electron density values were further analyzed.

The number and type of molecular interactions between the cellulose Iβ crystallite and each oligolignol-adhesive, was reported through the histogram shown in Fig. 7, under the following descriptions: blue columns correspond to the CA_βO4_SA_β5_CA trilignol (Complex 1), green columns for CA_βO4_SA_ββ_SA trilignol (Complex 2), yellow columns for SA_βO4_SA_ββ_SA trilignol (Complex 3), and red columns CA_ββ_CA dilignol (Complex 4). The non-covalent interactions found in each complex were classified as indicated above, i.e., $_{adh}OH\cdots O_{Cell}$, $_{adh}O\cdots HO_{Cell}$, $_{adh}CH\cdots O_{Cell}$, $_{adh}O\cdots HC_{Cell}$, and $_{adh}C\pi\cdots HC_{Cell}$ (or $_{adh}C\pi H\cdots O_{Cell}$).

Figure 7. Summary of non-covalent interactions found in the four oligolignol-cellulose complexes.

Complexes 02 and 03 presented the highest number of interactions, whit hydrogen bonds of the type "$_{adh}CH\cdots O_{Cell}$" predominating for Complex 3, while "$_{adh}O\cdots HC_{Cell}$" hydrogen bonds were more prevalent in Complex 2. Despite that Complex 2 (CA_βO4_SA_ββ_SA-cellulose Iβ) shows only three interactions namely O···HO, it also has a larger number of CH···O interactions, which can be associated with the largest YM value (Sedano-Mendoza, Lopez-Albarran & Pizzi, 2010b). Indeed, in this complex, a larger localized distribution of non-covalent interactions was found, while in Complex 3, predominant methyl hydrogen bonds were observed. From a molecular level description, this result elucidates which oligolignol promotes adhesion over cellulose, revealing the atomistic interactions involved in the oligolignol-cellulose complex based on the NCI-AIM study. The oligolignol CA_ββ_CA occurred in Complex 4, where it couples a guaiacyl fragment on the cellulose in a coplanar configuration, yielding closer intermolecular non-covalent interactions per dilignol coupled on the cellulose. In other words, weak interactions with density values larger than 0.003 a.u. are observed in this complex (Table S4). Interestingly, Complex 4 is reported as the second-best lignin substructure contributing to the adhesion.

Clearly, the CH···O interaction predominates over OH···O and CπH···O interactions, as displayed in Table S4. Thus, weak interactions like the CH···O contact hold significant relevance in binding oligolignols with cellulose, despite the fact that the larger interaction present only has a value of 0.023 a.u.; a phenomenon previously noted in analogous systems (Vargas et al., 2000a,b; Salazar-Cano et al., 2016). This aligns with the findings of several authors (Cintrón, Johnson & French, 2011; Huang et al., 2021) who suggest the important role of weak interactions over strong hydrogen bonds.

As mentioned earlier, neither stronger hydrogen bonds nor the quantity of weak interactions can be directly related to experimental values of the Young's modulus. Therefore, there seems to be a reciprocal influence between such interactions at the coupling of oligolignol. For instance, a substantial presence of strong hydrogen bonds, as observed in Complex 1, may give raise to regions with non-localized interactions. Conversely, a significant number of localized yet predominantly weak interactions, exemplified by Complex 3, might lead to a fragile support structure for oligolignol. In this context, the impact of each non-covalent interaction on the adhesion of oligolignols to cellulose was assessed by establishing causal relationships with the experimental YM values. Firstly, we plotted the average electronic density resulting from the $_{adh}CH\cdots O_{Cell}$ interaction against the experimental YM values (refer to Fig. 8), achieving a correlation factor of $R^2 = 0.97$.

Figure 8. Correlation between the average electron density of the $_{adh}CH\cdots O_{Cell}$ interactions and Young's modulus for the evaluated complexes.

In Fig. 8, it is evident that the larger the average electron density of the $_{adh}CH\cdots O_{Cell}$, the lower the Young's modulus. Interestingly, the $_{adh}CH\cdots O_{Cell}$ interactions observed in Complex 1 and Complex 3 result in larger values of the α angle (Table S1 and Table S3). Consequently, the adhesive components must adjust their positions to establish the particular $_{adh}CH\cdots O_{Cell}$ interaction, which could promote the formation of other crucial interactions. Furthermore, by plotting the total contribution of the $_{adh}XH\cdots O_{Cell}$ interactions (with X as C, Cπ and O atoms from oligolignols), against YM values, a linear correlation was also found ($R^2 = 0.79$), as depicted in Fig. 9. Interestingly, the slope of the aforementioned linear correlations was negative, indicating that such interactions limit the stretchability of the adhesive or achieves a rigid state, as suggested by Huang et al.(Huang et al., 2021) in the evaluation of mechanical properties of polymers.

Figure 9. Correlation obtained between the total electron density contribution of $_{adh}XH\cdots O_{Cell}$ interactions and Young's modulus for the evaluated complexes.

In contrast, plotting the total contribution of the weak interactions (interactions with electron density values below 0.005 a.u.) against the YM values yielded a positive slope and a correlation factor of $R^2 = 0.82$, as shown in Fig. 10. This significant correlation suggests that weak interactions play a fundamental role in enhancing adhesion by providing stabilization along the complex. Surprisingly, these linear correlations represent the first report to render the effect of non-covalent interactions on the mechanical parameter YM.

Figure 10. Correlation obtained between the total electron density contribution of weak interactions ($\rho \leq 0.005$ a.u.) and Young's modulus for the evaluated complexes.

Finally, by evaluating the ratio of the total contribution from $_{adh}XH\cdots O_{Cell}$ to the total contribution of weak interactions, a significant correlation ($R^2 = 0.87$) was also found, as shown in Fig. 11. This correlation, with a negative slope, suggests that better oligolignol adhesives can be obtained if both contributions are comparable, in agreement with the observations from Fig. 10. Accordingly, hydrogen bonds and weak interactions must play a complementary role in synthesizing better and environmentally friendly lignin-based adhesives.

Figure 11. Correlation obtained between the ratio of total electron density contribution of $_{adh}XH\cdots O_{Cell}$ and weak interactions and Young's modulus for the evaluated complexes.

It is noteworthy that the adhesion between cellulose and the best depolymerized lignin adhesive-formulation, can be elucidate from molecular modeling studies, considering an atomistic point of view where only one molecule of oligolignol interacts with the cellulose model. However, the experimental data were considered in assays where the solvents (mainly water) were removed by heating until the lignin adhesive formulations reached their Young's modulus.

Conclusions

Based on the established correlation between molecular dynamic interaction energy and Young's modulus (López-Albarrán et al., 2017), the trilignol CA_βO4_SA_ββ_SA and the dilignol CA_ββ_CA were identified as the lignin substructures contributing to the adhesion. These oligolignols exhibited favorable non-covalent interactions in this NCI-AIM study. Consequently, the adhesion between lignin-based adhesives and cellulose can be screened from specific non-covalent interactions between oligolignols and the cellulose model.

The coupling of oligolignols such as CA_βO4_SA_β5_CA on the cellulose Iβ surface induces the folding of the trilignol, resulting in extensive green (weak) isosurfaces associated with non-localized interactions. This contrasts with the CA_ββ_CA-cellulose Iβ complex.

Deciphering the precise contribution of each non-covalent interaction to the binding energy is challenging. Nevertheless, to provide insights into this aspect, the roles of various oligolignol-cellulose interactions were described. Notably, C-H···O contacts were prevalent, with oligolignols serving as hydrogen atom donors in some instances and cellulose acting as the donor in others. Furthermore, weak interactions such as the CH···O contact played a significant role in binding oligolignols with cellulose. Examining the electron density of the H-bonds $_{adh}XH\cdots O_{Cell}$ and weak interactions revealed their complementary roles in fully describing the adhesive phenomenon. A paradigmatic relationship was observed, the linear correlations established in this study represent the first report demonstrating the influence of non-covalent interactions on the measurable mechanical parameter YM. Our findings indicate that non-covalent interactions control the forces associated to adhesive-cellulose contacts, primarily through C-H···O hydrogen bonds, which promote the adhesion of oligolignols on cellulose Iβ. Results indicate that the adhesion strength projected from larger YM values cannot be describe solely by the number of stronger hydrogen bonds nor by the number of the weak interactions but by the entire contributions of specific interactions.

Additional Information and Declarations

The following information was supplied regarding data availability: The interaction correlations from raw data and the scripting code for figures are available in the Supplemental Files Data S1-S6.

Acknowledgements

Thanks to CIC-UMSNH for financial support under grant Convocatoria CIC 2023, and the CONAHCYT for financial support in "Estancia Sabática Nacional 2022-2023". Also, the authors appreciate the suggestions from Andrea López-Martinez.

References

Antov P, Savov V, Neykov N. 2020. Sustainable bio-based adhesives for eco-friendly wood composites. A review. Wood Res 65:51–62.

Bader RFW, Nguyen-Dang TT. 1981. Quantum Theory of Atoms in Molecules–Dalton Revisited. Advances in Quantum Chemistry 14. DOI: 10.1016/S0065-3276(08)60326-3.

Besombes S, Mazeau K. 2005. The cellulose/lignin assembly assessed by molecular modeling. Part 1: Adsorption of a threo guaiacyl β-O-4 dimer onto a Iβ cellulose whisker. Plant Physiology and Biochemistry 43:299–308. DOI: 10.1016/j.plaphy.2005.02.005.

Boto RA, Contreras-García J, Tierny J, Piquemal JP. 2016. Interpretation of the reduced density gradient. Molecular Physics 114:1406–1414. DOI: 10.1080/00268976.2015.1123777.

Chenoweth K, Van Duin ACT, Goddard WA. 2008. ReaxFF reactive force field for molecular dynamics simulations of hydrocarbon oxidation. The Journal of Physical Chemistry A 112:1040–1053.

Cintrón MS, Johnson GP, French AD. 2011. Young's modulus calculations for cellulose Iβ by MM3 and quantum mechanics. Cellulose 18:505–516. DOI: 10.1007/s10570-011-9507-1.

Dapprich S, Komáromi I, Byun KS, Morokuma K, Frisch MJ. 1999. A new ONIOM implementation in Gaussian98. Part I. The calculation of energies, gradients, vibrational frequencies and electric field derivatives. Journal of Molecular Structure: THEOCHEM 461:1–21.

Desai SD, Patel J V, Sinha VK. 2003. Polyurethane adhesive system from biomaterial-based polyol for bonding wood. International Journal of Adhesion and Adhesives 23:393–399.

Djahedi C, Bergenstråhle-Wohlert M, Berglund LA, Wohlert J. 2016. Role of hydrogen bonding in cellulose deformation: the leverage effect analyzed by molecular modeling. Cellulose 23:2315–2323. DOI: 10.1007/s10570-016-0968-0.

Fengel D, Wegener G. 1983. Wood: chemistry, ultrastructure, reactions. Walter de Gruyter.

Frisch MJ, Trucks GW, Schlegel HB, Scuseria GE, Robb MA, Cheeseman JR, Scalmani G, Barone V, Petersson GA, Nakatsuji H, Li X, Caricato M, Marenich A V, Bloino J, Janesko BG, Gomperts R, Mennucci B, Hratchian HP, Ortiz J V, Izmaylov AF, Sonnenberg JL, Williams-Young D, Ding F, Lipparini F, Egidi F, Goings J, Peng B, Petrone A, Henderson T, Ranasinghe D, Zakrzewski VG, Gao J, Rega N, Zheng G, Liang W, Hada M, Ehara M, Toyota K, Fukuda R, Hasegawa J, Ishida M, Nakajima T, Honda Y, Kitao O, Nakai H, Vreven T, Throssell K, Montgomery Jr. JA, Peralta JE, Ogliaro F, Bearpark MJ, Heyd JJ, Brothers EN, Kudin KN, Staroverov VN, Keith TA, Kobayashi R, Normand J, Raghavachari K, Rendell AP, Burant JC, Iyengar SS, Tomasi J, Cossi M, Millam JM, Klene M, Adamo C, Cammi R, Ochterski JW, Martin RL, Morokuma K, Farkas O, Foresman JB, Fox DJ. 2016. Gaussian16 Revision C.01.

Gomes TCF, Skaf MS. 2012. Cellulose-Builder: A toolkit for building crystalline structures of cellulose. Journal of computational chemistry 33:1338–1346.

513 Grimme S. 2004. Accurate description of van der Waals complexes by density functional theory
514 including empirical corrections. Journal of Computational Chemistry 25:1463–1473.
515 Hernández-Esparza R, Mejía-Chica SM, Zapata-Escobar AD, Guevara-García A, Martínez-
516 Melchor A, Hernández-Pérez JM, Vargas R, Garza J. 2014. Grid-based algorithm to search
517 critical points, in the electron density, accelerated by graphics processing units. Journal of
518 Computational Chemistry 35:2272–2278. DOI: 10.1002/jcc.23752.
519 Houtman CJ, Atalla RH. 1995. Cellulose-lignin interactions (A computational study). Plant
520 physiology 107:977–984.
521 Huang X, Nakagawa S, Houjou H, Yoshie N. 2021. Insights into the Role of Hydrogen Bonds on
522 the Mechanical Properties of Polymer Networks. Macromolecules 54:4070–4080. DOI:
523 10.1021/acs.macromol.1c00120.
524 Imam SH, Gordon SH, Mao L, Chen L. 2001. Environmentally friendly wood adhesive from a
525 renewable plant polymer: characteristics and optimization. Polymer Degradation and Stability
526 73:529–533.
527 Ishikawa T, Hayakawa D, Miyamoto H, Ozawa M, Ozawa T, Ueda K. 2015. Ab initio studies on
528 the structure of and atomic interactions in cellulose IIII crystals. Carbohydrate Research 417:72–
529 77. DOI: https://doi.org/10.1016/j.carres.2015.09.006.
530 Jin Y, Cheng X, Zheng Z. 2010. Preparation and characterization of phenol–formaldehyde
531 adhesives modified with enzymatic hydrolysis lignin. Bioresource Technology 101:2046–2048.
532 Johnson ER, Keinan S, Mori-Sanchez P, Contreras-Garcia J, Cohen AJ, Yang W. 2010b.
533 Revealing noncovalent interactions. Journal of the American chemical society 132:6498–6506.
534 Jurečka P, Šponer J, Černý J, Hobza P. 2006. Benchmark database of accurate (MP2 and
535 CCSD(T) complete basis set limit) interaction energies of small model complexes, DNA base
536 pairs, and amino acid pairs. Physical Chemistry Chemical Physics 8:1985–1993. DOI:
537 10.1039/B600027D.
538 Kendall RA, Dunning Jr TH, Harrison RJ. 1992. Electron affinities of the first-row atoms
539 revisited. Systematic basis sets and wave functions. The Journal of Chemical Physics 96:6796–
540 6806.
541 Knop A, Scheib W. 1979. Chemistry and application of phenolic resins. Springer.
542 Koch U, Popelier PLA. 1995. Characterization of CHO hydrogen bonds on the basis of the
543 charge density. The Journal of Physical Chemistry 99:9747–9754.
544 Kohn W, Becke AD, Parr RG. 1996. Density Functional Theory of Electronic Structure. The
545 Journal of Physical Chemistry 100:12974–12980. DOI: 10.1021/jp960669l.
546 Li K, Geng X, Simonsen J, Karchesy J. 2004. Novel wood adhesives from condensed tannins
547 and polyethylenimine. International Journal of Adhesion and Adhesives 24:327–333.
548 López-Albarrán P, Pizzi A, Navarro-Santos P, Hernández-Esparza R, Garza J. 2017.
549 Oligolignols within lignin-adhesive formulations drive their Young's modulus: A ReaxFF-MD
550 study. International Journal of Adhesion and Adhesives 78:227–233. DOI:
551 10.1016/j.ijadhadh.2017.08.003.

Mansouri HR, Navarrete P, Pizzi A, Tapin-Lingua S, Benjelloun-Mlayah B, Pasch H, Rigolet S. 2011. Synthetic-resin-free wood panel adhesives from mixed low molecular mass lignin and tannin. European Journal of Wood and Wood Products 69:221–229.

Martinez C, Sedano M, Munro A, Lopez P, Pizzi A. 2010. Evaluation of Some Synthetic Oligolignols as Adhesives: A Molecular Docking Study. Journal of Adhesion Science and Technology 24:1739–1751. DOI: 10.1163/016942410x507803.

Momma K, Izumi F. 2008. VESTA: A three-dimensional visualization system for electronic and structural analysis. Journal of Applied Crystallography 41:653–658. DOI: 10.1107/S0021889808012016.

Moon RJ, Martini A, Nairn J, Simonsen J, Youngblood J. 2011. Cellulose nanomaterials review: structure, properties and nanocomposites. Chemical Society Reviews 40:3941–3994. DOI: 10.1039/C0CS00108B.

Navarrete P, Mansouri HR, Pizzi A, Tapin-Lingua S, Benjelloun-Mlayah B, Pasch H, Rigolet S. 2010. Wood panel adhesives from low molecular mass lignin and tannin without synthetic resins. Journal of Adhesion Science and Technology 24:1597–1610.

Navarrete-López AM, Garza J, Vargas R. 2007. Relationship between the critical points found by the electron localization function and atoms in molecules approaches in adducts with hydrogen bonds. The Journal of Physical Chemistry A 111:11147–11152.

Navarrete-López AM, San-Román ML, Zicovich-Wilson CM. 2016. The influence of the DFT approach on the structure and relative stability of models for cellulose I allomorphs. Theoretical Chemistry Accounts 135:1–13.

Nimz H. 1983. Lignin-based wood adhesives. In: Pizzi A ed. Wood adhesion chemistry and technology. New York: Dekker, 247–288.

Nishiyama Y, Langan P, Chanzy H. 2002a. Crystal structure and hydrogen-bonding system in cellulose Iβ from synchrotron X-ray and neutron fiber diffraction. Journal of the American chemical society 124:9074–9082.

Nishiyama Y, Sugiyama J, Chanzy H, Langan P. 2003. Crystal structure and hydrogen bonding system in cellulose Iα from synchrotron X-ray and neutron fiber diffraction. Journal of the American chemical society 125:14300–14306.

Pizzi A. 1994. Advanced wood adhesives technology. CRC Press.

Pizzi A. 2006. Recent developments in eco-efficient bio-based adhesives for wood bonding: opportunities and issues. Journal of Adhesion Science and Technology 20:829–846.

Pizzi A. 2013. Bioadhesives for wood and fibres. Reviews of Adhesion and Adhesives 1:88–113.

Pizzi A, Mittal KL. 2011. Wood adhesives. CRC Press.

Pizzi A, Mittal KL, Sedano-Mendoza M, Lopez-Albarran P, Pizzi A. 2011. Natural Lignans as Adhesives for Cellulose. In: Wood Adhesives. CRC Press, 3–20.

Ponnuchamy V, Sandak A, Sandak J. 2020. Multiscale modelling investigation of wood modification with acetic anhydride. Phys. Chem. Chem. Phys. 22:28448–28458. DOI: 10.1039/D0CP05165A.

591 Rappé AK, Casewit CJ, Colwell KS, Goddard Iii WA, Skiff WM. 1992. UFF, a full periodic
592 table force field for molecular mechanics and molecular dynamics simulations. Journal of the
593 American chemical society 114:10024–10035.
594 Salazar-Cano J-R, Guevara-García A, Vargas R, Restrepo A, Garza J. 2016. Hydrogen bonds in
595 methane–water clusters. Physical Chemistry Chemical Physics 18:23508–23515.
596 Sedano-Mendoza M, Lopez-Albarran P, Pizzi A. 2010a. Natural lignans as adhesives for
597 cellulose: Computational interaction energy vs experimental results. Journal of Adhesion Science
598 and Technology 24:1769–1786. DOI: 10.1163/016942410X507777.
599 Shimada M, Higuchi T. 1983. Recent advances in lignin biodegradation research. Recents
600 advances in lignin biodegradation research. T. Higuchi, HM Chang y TK Kirk (Eds.), Uni
601 Publishers. Tokio:195–208.
602 Sjöström E. 1998. Analytical methods in wood chemistry, pulping, and papermaking. Springer.
603 Terashima N, Nakashima J, Takabe K. 1998. Proposed Structure for Protolignin in Plant Cell
604 Walls. In: ACS Symposium Series. Oxford University Press, 180–193. DOI: 10.1021/bk-1998-
605 0697.ch014.
606 Ultra C. 2007. 11.0. 1. CambridgeSoft Corporation, Cambridge.
607 Vargas R, Garza J, Dixon DA, Hay BP. 2000a. How Strong Is the Cα−H···OC Hydrogen Bond?
608 Journal of the American Chemical Society 122:4750–4755. DOI: 10.1021/ja993600a.
609 Vargas R, Garza J, Dixon DA, Hay BP. 2000b. Conformational Analysis of N,N,N‘,N‘-
610 Tetramethylsuccinamide: The Role of C−H···O Hydrogen Bonds. The Journal of Physical
611 Chemistry A 104:5115–5121. DOI: 10.1021/jp000030o.
612 Vreven T, Morokuma K. 2006. Chapter 3 Hybrid Methods: ONIOM(QM:MM) and QM/MM.
613 Annual Reports in Computational Chemistry 2:35–51. DOI: 10.1016/S1574-1400(06)02003-2.
614 Yanai T, Tew DP, Handy NC. 2004. A new hybrid exchange–correlation functional using the
615 Coulomb-attenuating method (CAM-B3LYP). Chemical Physics Letters 393:51–57.
616 Zhao Y, Truhlar DG. 2008. The M06 suite of density functionals for main group
617 thermochemistry, thermochemical kinetics, noncovalent interactions, excited states, and
618 transition elements: two new functionals and systematic testing of four M06-class functionals
619 and 12 other function. Theoretical Chemistry Accounts 120:215–241.

Figure 1

Lignin precursors.

Lignin precursors. (A) p-coumarol, (B) coniferol, and (C) sinapol, all of them showed in their predominant (E)-monolignol configuration. Carbon numbering is shown on the coniferol structure.

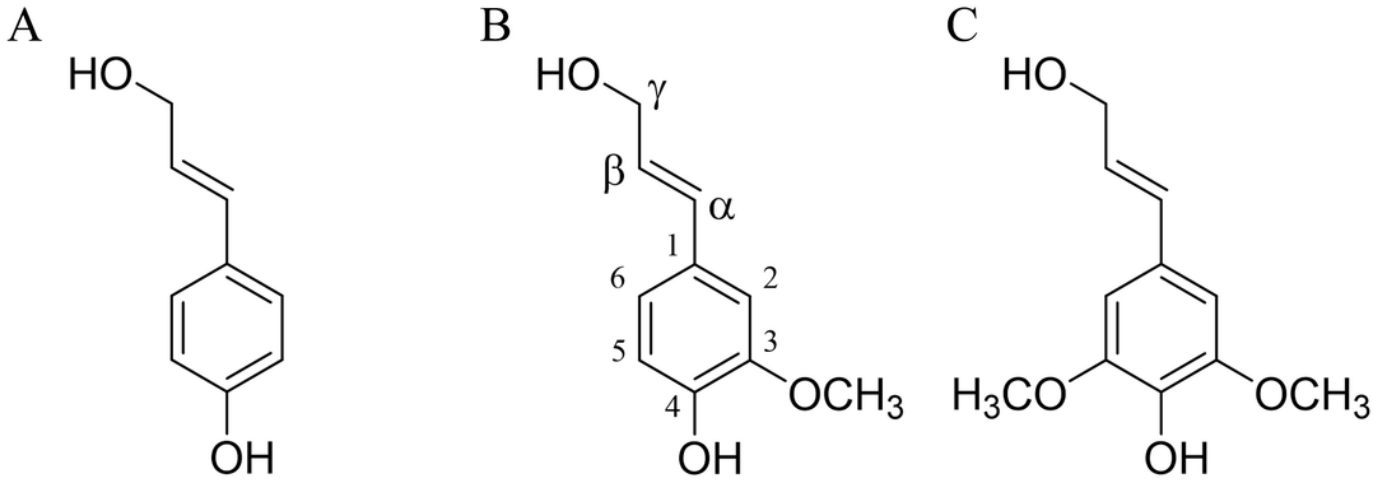

Figure 2

Snapshot of the cellulose Iβ model used to form the complexes with the oligolignols.

The model was built using the Cellulose-Builder toolkit, [(Gomes & Skaf, 2012)] and visualized by the Vesta molecular viewer. [(Momma & Izumi, 2008)] Color key: carbons atoms are in dark-gray, oxygen atoms in red, and hydrogen atoms in white.

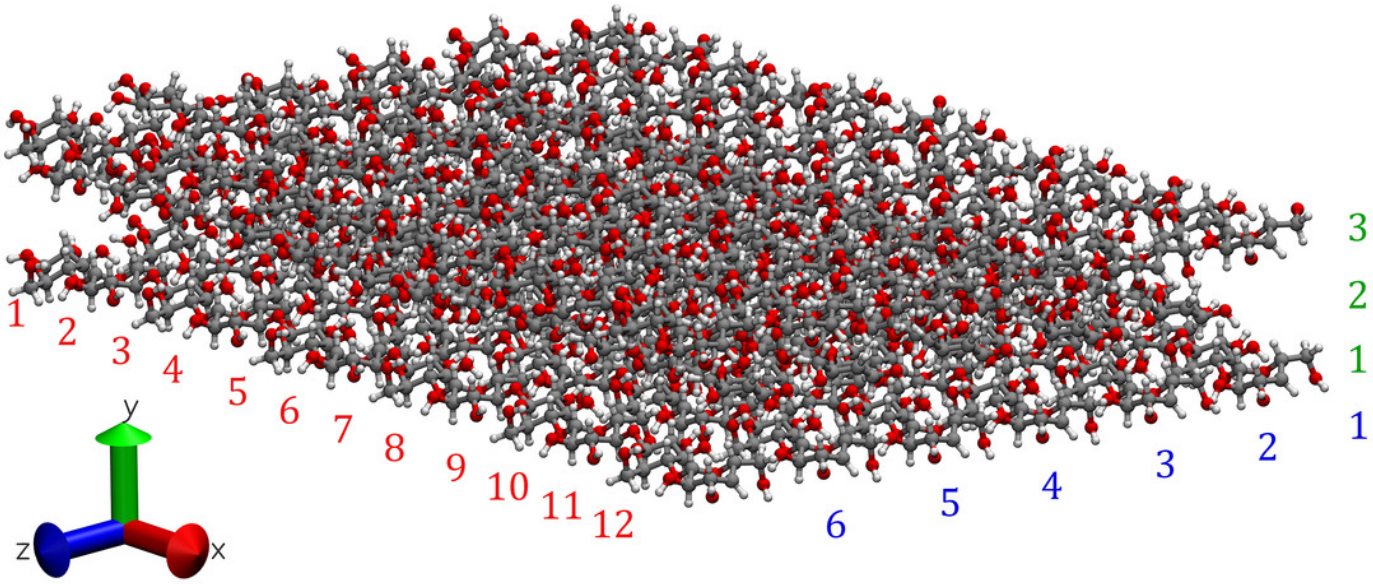

Figure 3

Molecular structures of the oligolignols

Molecular structures of the oligolignols in the reported efficient adhesive formulation. (A) CA_βO4_SA_β5_CA, (B) CA_βO4_SA_ββ_SA, (C) SA_βO4_SA_ββ_SA, and (D) CA_ββ_CA.

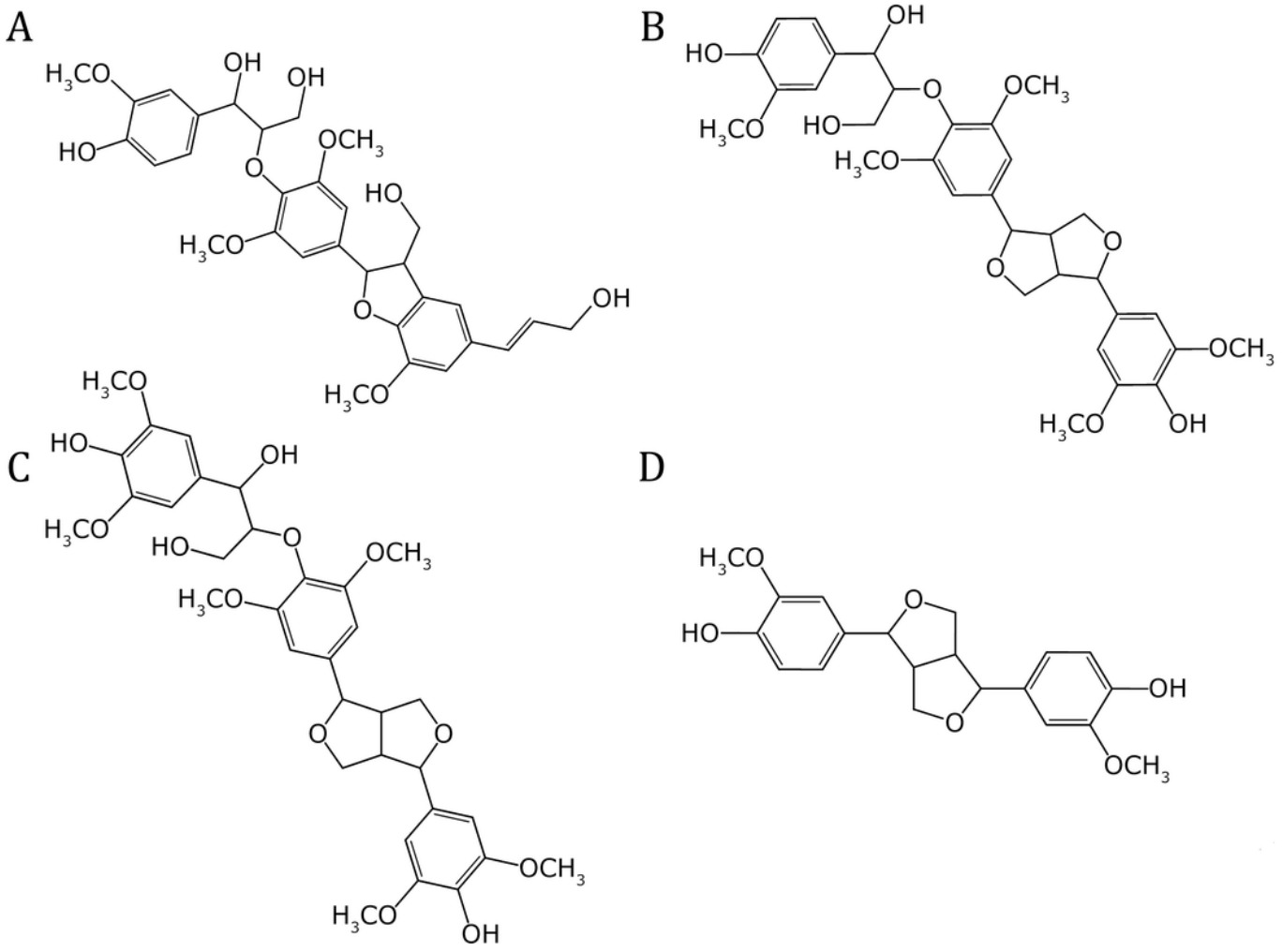

Figure 4

Superposition of the four oligolignols complexed over the cellulose Iβ crystallite model.

Superposition of the four oligolignols complexed over the cellulose Iβ crystallite model. For convenience the cellulose Iβ surface is not present in this figure however, this part of the system was considered in the QM/MM optimization process. The complex conformations obtained from the LAMMPS-ReaxFF-MD are in green carbon-skeleton, and the QM/MM-CAM-B3LYP (Yanai, Tew & Handy, 2004) /cc-pVDZ (Kendall, Dunning Jr & Harrison, 1992) /Universal Force Field (Rappé et al., 1992) (UFF) are in purple carbon-skeleton. (A) CA_*βO4*_SA_*β5*_CA trilignol, (B) CA_*βO4*_SA_*ββ*_SA trilignol, (C) SA_*βO4*_SA_*ββ*_SA trilignol, and (D) CA_*ββ*_CA dilignol.

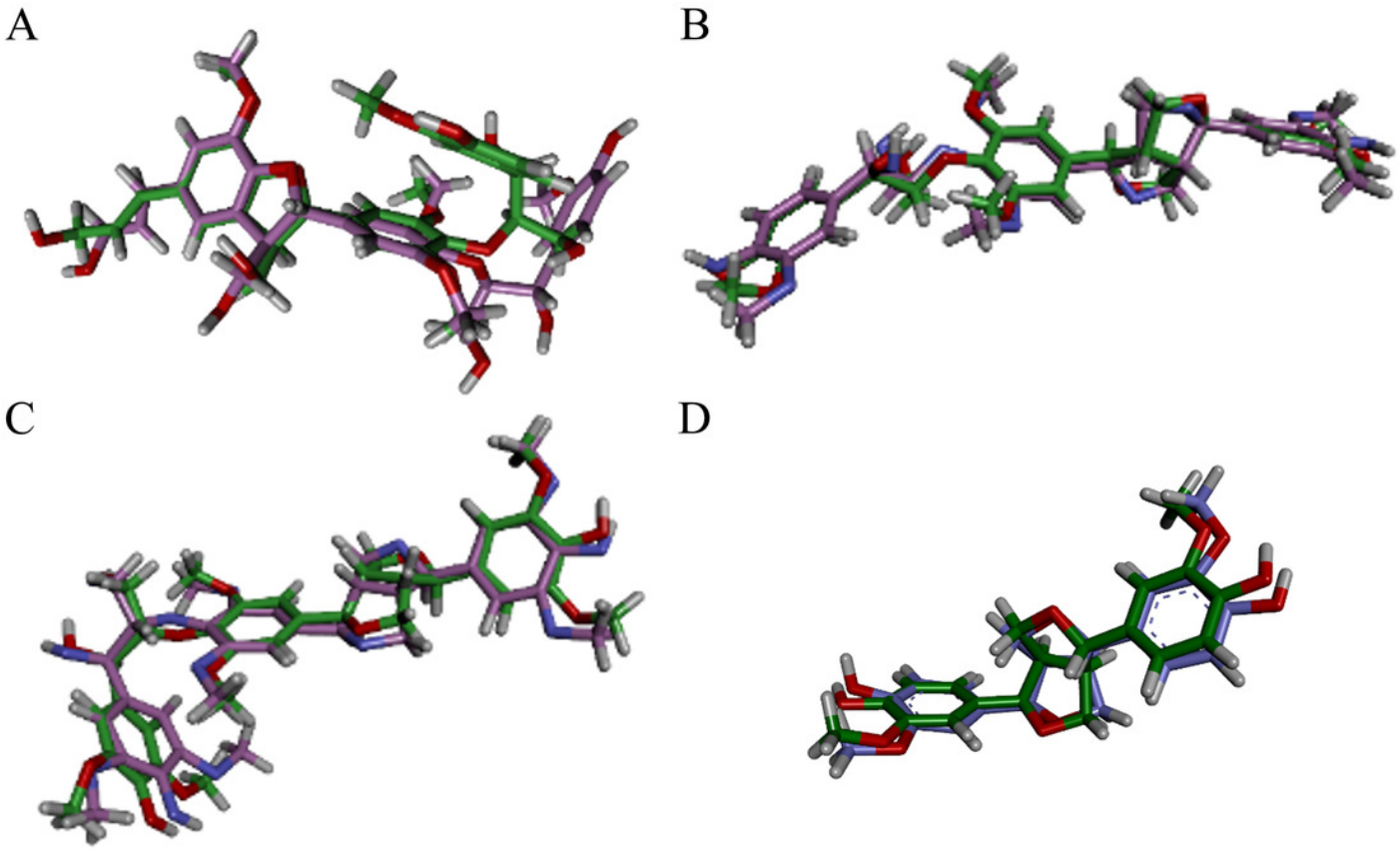

Figure 5

Mapping of the NCI-AIM surfaces and plot of reduced electron density gradient (RDG) against Sign(λ_2)

Mapping of the NCI-AIM surfaces and plot of reduced electron density gradient (RDG) against Sign(λ_2)ρ. (A) Complex 1, CA_*βO4*_SA_*β5*_CA– cellulose Iβ; (B) Complex 2, CA_*βO4*_SA_*ββ*_SA–cellulose Iβ; (C) Complex 3, SA_*βO4*_SA_*ββ*_SA–cellulose Iβ; (D) Complex 4, CA_*ββ*_CA–cellulose Iβ. Blue regions are for hydrogen bonds, green regions for van der Waals. The gradient isosurfaces correspond to a cutoff of 0.5 a.u. Color scale ranging from <!--[if !msEquation]--> <!--[if !vml]--> <!--[endif]--><!--[endif]--> a.u. The interactions labeled as **a**-**u** (if exist) corresponded to the interactions indicated in Tables S1-S4.

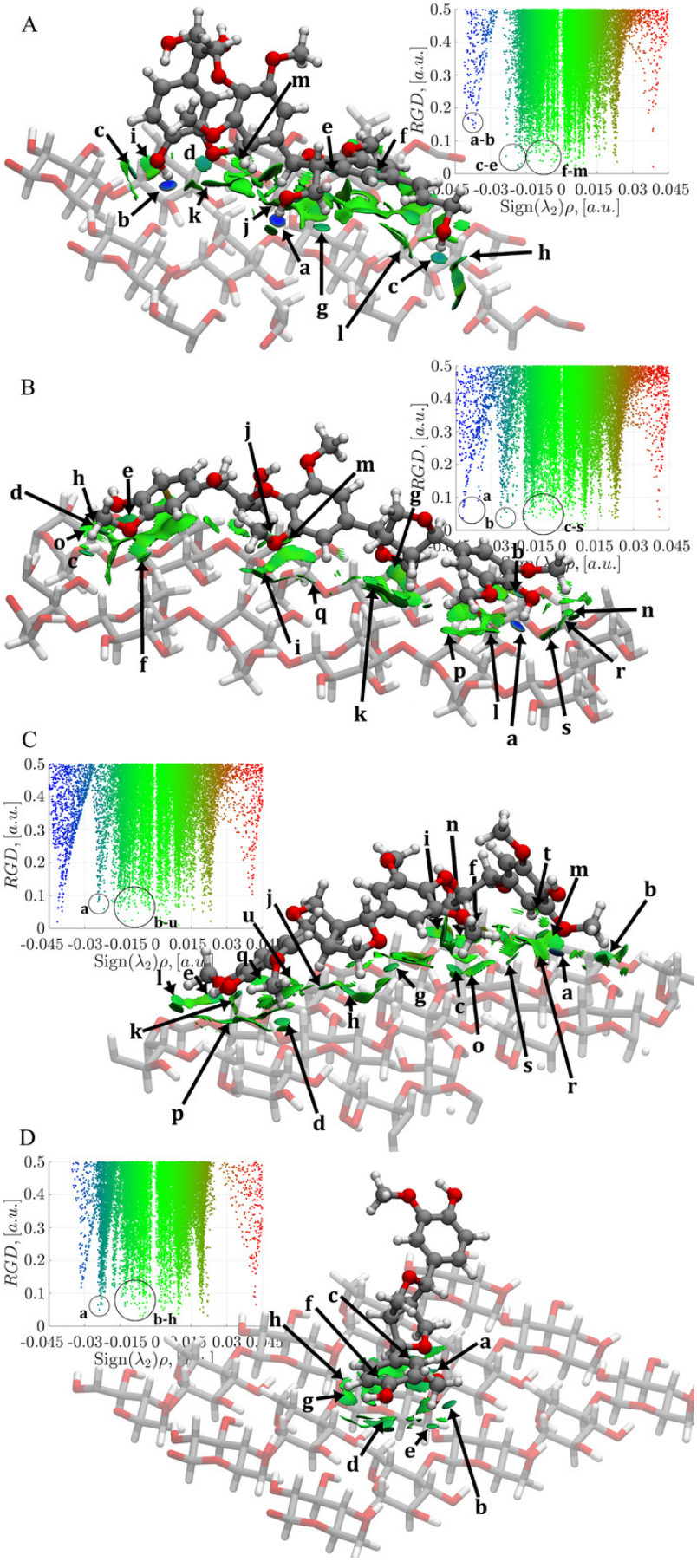
A
B
C
D
RGD, [a.u.]
Sign(λ_2)ρ, [a.u.]
a-b
c-e
f-m
c-s
b-u
b-h

Figure 6

Illustration of the main hydrogen bond based on electronic density isovalues

Illustration of the main hydrogen bond based on electronic density isovalues and a blue code color: ρ(r)≥0.02 in dark blue, 0.01≤ρ(r)<0.02 in blue and ρ(r)<0.01 in cyan.(Johnson et al., 2010b) Atoms involved in hydrogen bond are highlighted in magenta. (A) Complex 1, CA_βO4_SA_β5_CA – cellulose Iβ; (B) Complex 2, CA_βO4_SA_ββ_SA – cellulose Iβ; (C) Complex 3, SA_βO4_SA_ββ_SA – cellulose Iβ; (D) Complex 4, CA_ββ_CA – cellulose Iβ.

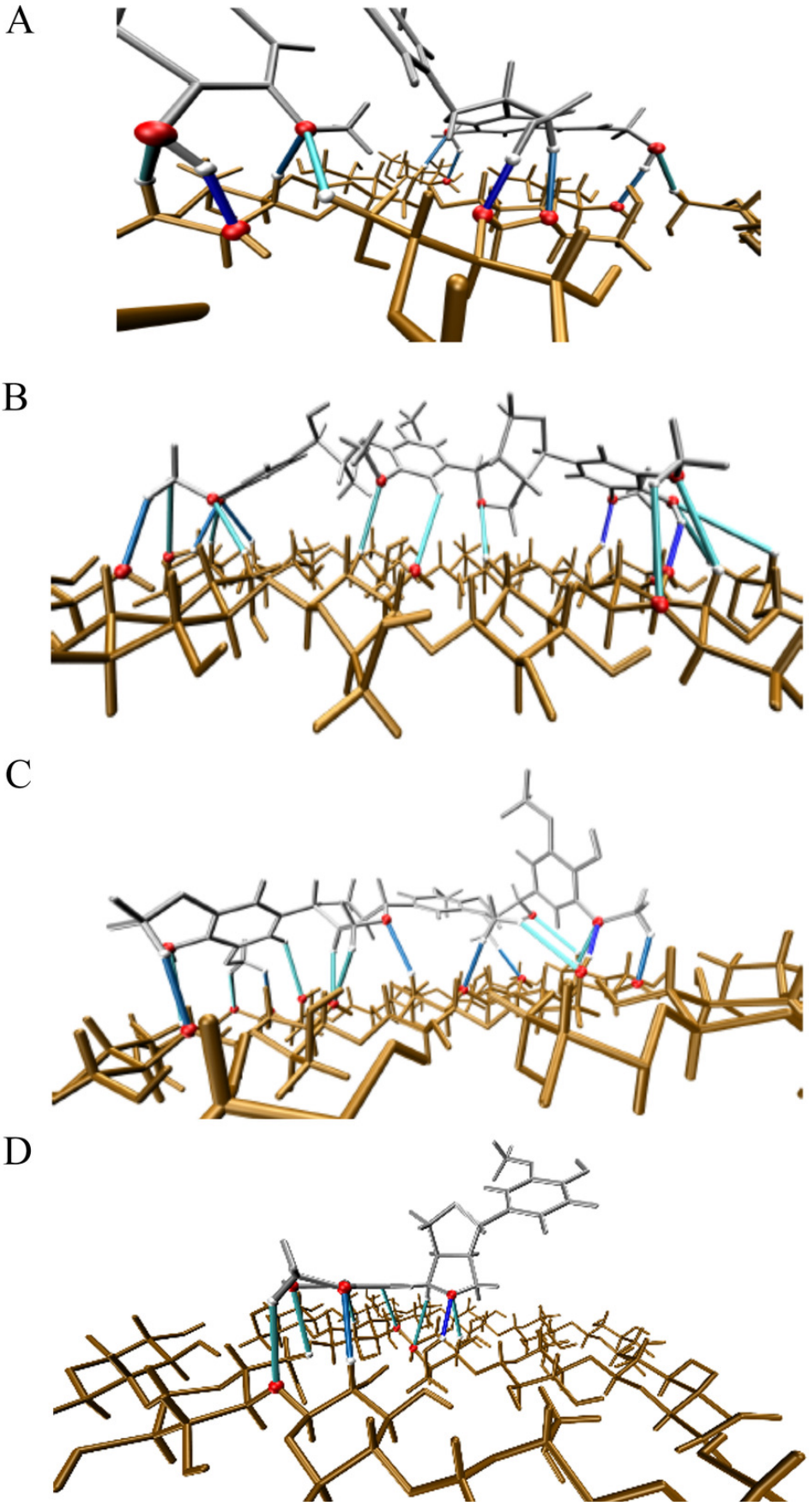
A
B
C
D

Figure 7

Summary of non-covalent interactions

Summary of non-covalent interactions found in the four oligolignol-cellulose complexes.

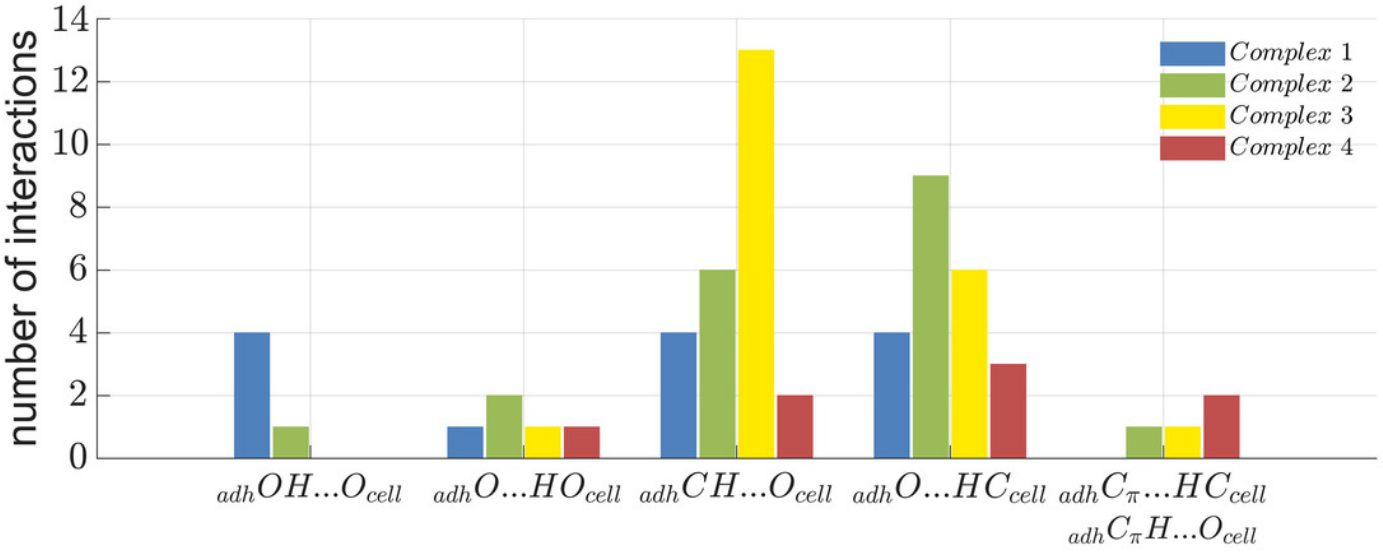

Figure 8

Linear correlation between $_{adh}CH\cdots O_{Cell}$ interactions and Young's modulus

Correlation between the average electron density of the $_{adh}CH\cdots O_{Cell}$ interactions and Young's modulus for the evaluated complexes.

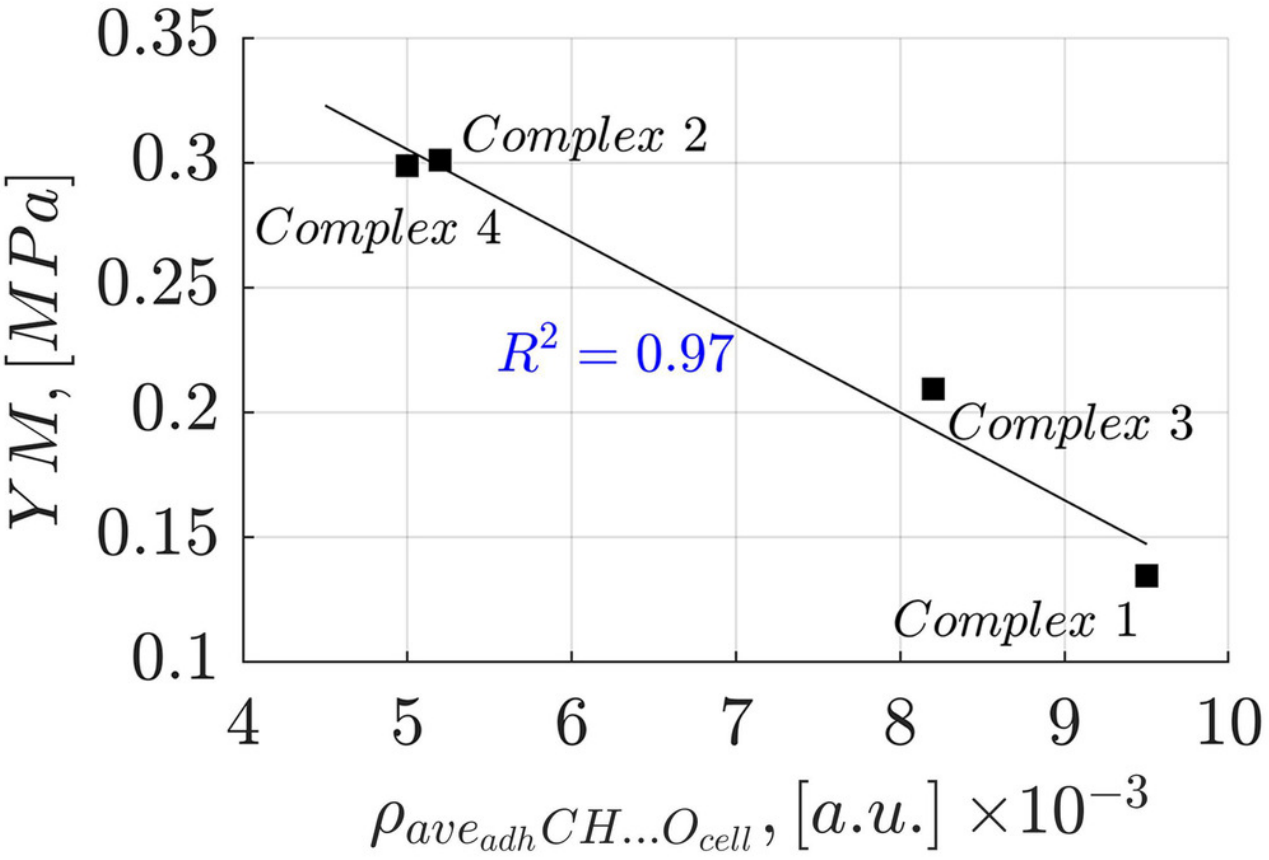

Figure 9

Linear correlation between $_{adh}XH\cdots O_{Cell}$ interactions and Young's modulus

Correlation obtained between the total electron density contribution of $_{adh}XH\cdots O_{Cell}$ interactions and Young's modulus for the evaluated complexes.

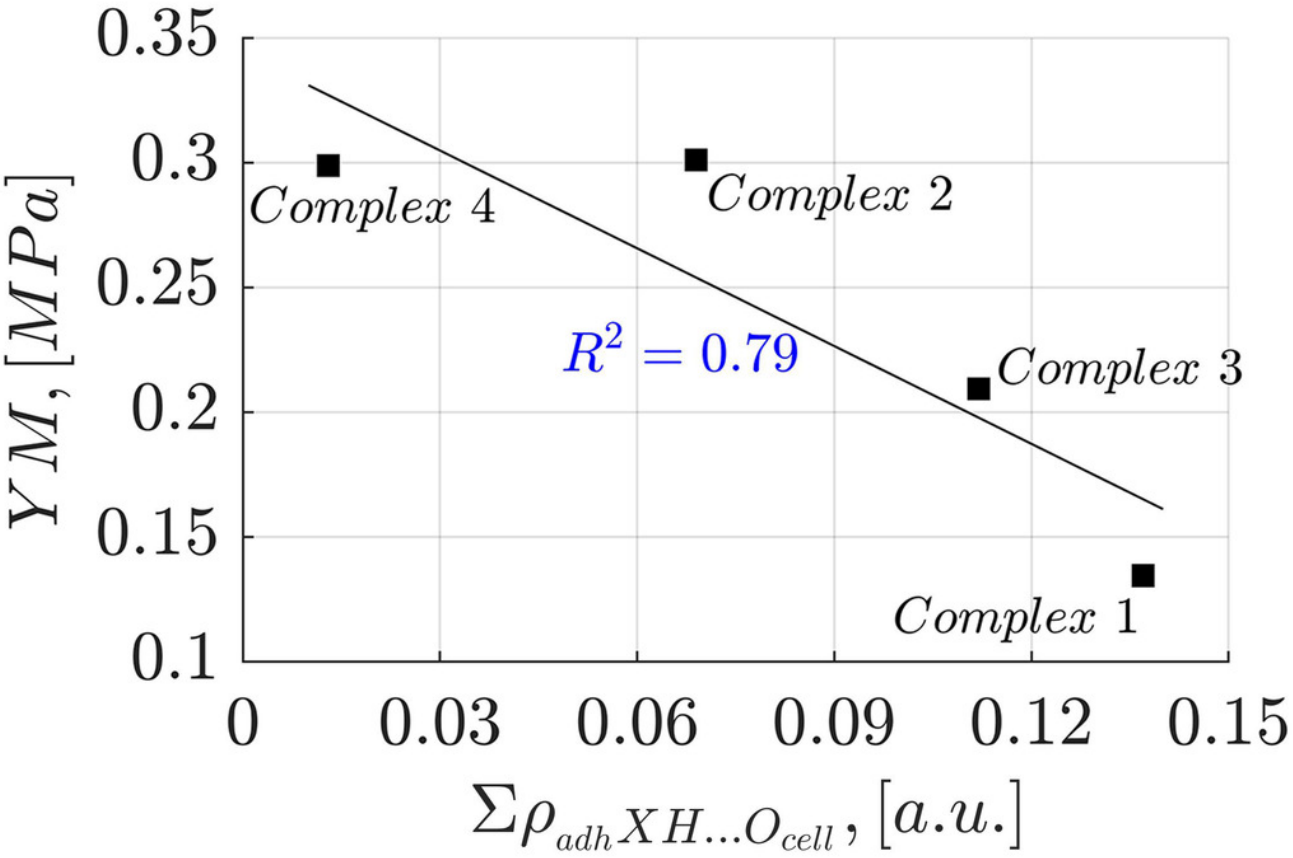

Figure 10

Linear correlation between weak interactions (ρ < 0.005 a.u.) and Young's modulus

Correlation between the total electron density contribution of weak interactions (ρ < 0.005 a.u.) and Young's modulus for the evaluated complexes.

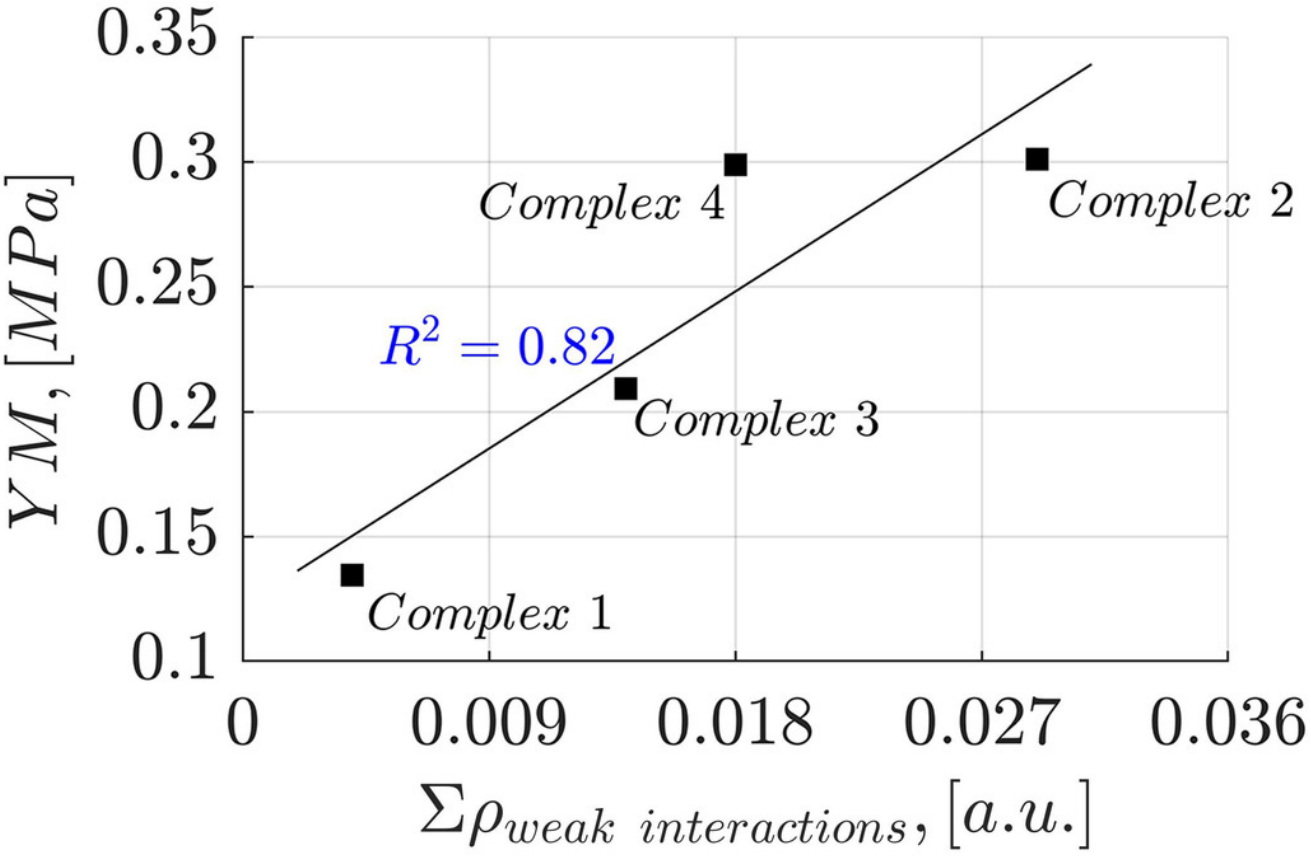

Figure 11

Correlation the ratio of $_{adh}XH\cdots O_{Cell}$ weak interactions and Young's modulus.

Correlation the ratio of total electron density contribution of $_{adh}XH\cdots O_{Cell}$ and weak interactions and Young's modulus for the evaluated complexes.